Shape-Based Optimization of a Plasma Etching Process

Jordan M. Berg and Nan Zhou
Department of Mechanical Engineering
Texas Tech University
Lubbock, TX 79409-1021
jordan.berg@ttu.edu

Abstract

This paper considers the problem of determining a finite number of discrete parameters appearing in a nonlinear partial differential equation describing a curve evolution process. The method is applied to the plasma etching of thin films for semiconductor manufacturing. Results are obtained within the mathematical framework of level set methods. Here, the evolution of the curve under study is captured through the evolution of a level set function. The underying physics of the process are completely contained in a scalar function called the speed function. The degree of difficulty of treating the evolution equation depends on the functional dependencies of the speed function. This paper presents optimal estimation and design techniques based on analytical gradient computations for a class of position and orientation dependent speed functions. The technique is demonstrated on a plasma etching model taken from the literature. Only simulation results are presented here, but the model under study has been shown to reproduce experimental data with reasonable accuracy. In the estimation problem, parameters in the model are fit to best match the feature shape measured in experiments. In the optimal design problem, parameter values are selected to most closely attain a desired feature shape.

1 Introduction

Although processes in which shape is the controlled output or measured quantity are of considerable economic importance, there are relatively few tools available for their estimation and control. Etching and deposition of surface features into thin films for fabrication of microelectronic devices are an example of such processes. This application is the subject of the present work, though the techniques described are general. Here the feature shape at the end of the etch or deposition can be considered to be the output of the process. An estimation problem might involve inferring information about the underlying physics from the observed shape. A control problem might consist of determining optimal values for user-specified process settings in order to achieve a desired shape. In order to proceed with either objective, a model is needed relating evolution of the shape to the process variables. In particular, this paper is concerned with techniques that combine functional models of the process with adjustable parameters that must be fit to data.

In such an approach, broad knowledge of the process physics is used to construct a low-order model. A sampling of models may be found in [7, 12, 21, 23, 24]. These models are well-suited to real-time or iterative applications, but their usefulness depends on the ability of the process engineer to choose the parameter values correctly. The values may be selected based on surface evolution data taken from scanning electron micrographs of feature cross-sections. For the most part, this calibration process is *ad hoc*, and relies heavily on the modeler's expert knowledge of the system; for examples see [8]. To our knowledge, only one study has investigated methods to optimize this process systematically [7]. That work, while successful, used a non-geometric cost function that requires the user to select points in one-to-one correspondence on the actual and estimated surfaces. The focus of this paper is selection of a cost function that does not depend on specifics of the nominal feature. Such a cost function may be obtained based on a *metric* for the space of shapes. Several choices of metrics have been proposed for the formalization of shape identification, and visual processing in general [13]. The one used here is the *template metric*, discussed further below.

This work uses level set methods to describe the feature evolution. Sethian and Adalsteinsson apply level set methods to the simulation of feature development in a variety of semiconductor manufacturing applications [17, 16], using numerical methods based on hyperbolic conservation laws [14].

Numerous papers have appeared on real-time control of plasma etching and deposition [6, 9, 11, 15, 20], but relatively few address events at the wafer surface, focusing instead on the bulk properties of the plasma. Those that do consider the wafer surface typically consider only planar processes [22]. Earlier work of the

PI and co-workers focused on developing techniques for *real-time* feature-level estimation and control of plasma etching [2]. The development of the gradient formulas used in the present work was begun in [1], and a limited application of these results was made to simple models of photolithographic development and plasma etching in [3]. The present work presents a complete scheme for computing gradients, and applies the results to a realistic plasma etching model, including such necessary effects as shadowing and non-uniform ion energy distribution. The model used was presented in a series of papers by Jurgensen, Shaqfeh, and co-workers [10, 18, 19]. They initially obtain a sputtering model that successfully reproduced experimental results from oxygen plasma ion-assisted etching (IAE) of silicon [18]. Ultimately they included isotropic etch and radical re-emission terms, producing a model that successfully matched sulfur hexaflouride IAE of silicon over a wide range of process parameters. The current paper incorporates the sputtering model and an isotropic term, but neglects re-emission. This is equivalent to the model of [19] with sticking coefficient equal to zero.

2 Level Sets

In this paper we restrict our attention to curves in the plane. Many aspects of our approach carry over to three dimensions directly, others will need some modification. However, a number of important problems may be treated effectively in two dimensions.

In the level set formulation, an oriented curve evolving in time, $\mathcal{C}(t)$ is represented by the zero level set (ZLS) of a level set function (LSF) $\Phi(x,t)$, that is, $\mathcal{C}(t) = \{x \in R^2 : \Phi(x) = 0\}$. The orientation is recovered by defining the points at which the LSF is negative as the interior, and requiring that the unit normal point outward. $\mathcal{C}(t)$ evolves in time according to $\mathcal{C}_t = \tilde{\alpha}(s,t,\ldots)\tau + \tilde{\beta}(s,t,\ldots)\nu$, where τ and ν are, respectively, the tangent and outward pointing normal unit vectors. Now the evolution of the LSF corresponding to $\mathcal{C}(t)$ is governed by the PDE $\Phi_t + \beta(x,t,\ldots)\|\nabla\Phi\| = 0$. Note that the component of the velocity along the tangent plays no part in the evolution of the LSF. Also note an important distinction between β and $\tilde{\beta}$. Namely, $\tilde{\beta}$ is defined only on $\mathcal{C}(t)$ itself, but β is a function on the entire plane. Of course on $\mathcal{C}(t)$, β must agree with $\tilde{\beta}$. For a derivation of this equation, or for more detail on its meaning when the LSF fails to be differentiable in space, see [16] and the references therein.

The process of parameter identification will require that we find the parameter values that give, in some sense, the closest match to an observed evolution. To make this rigorous, we must define a metric for LSFs that formalizes the idea of "distance." A number of appropriate metrics are discussed by Mumford [13]. All these are of potential interest, but here we consider only the *template metric*. We define the distance between two closed curves to be the area contained between them. That is, it is the total area that is inside of one of the curves, but outside the other. It is straightforward to compute the template metric when the estimate and the measurement curve are both characterized by LSFs. One way to make this calculation is to multiply the two LSFs pointwise. The result is a new LSF, which we call the *product LSF*. The ZLS of the product LSF defines a curve, and the area of the interior of this curve is exactly the error area. To compute the value of the metric we generate $\mathcal{C}_3$—the contour corresponding to the product LSF—and apply Green's theorem to obtain $\rho = \frac{1}{2}\int_{\mathcal{C}_3}\langle\mathcal{C}_3,\nu\rangle\,ds$, where $\langle\cdot,\cdot\rangle$ is the vector inner product, ν is the outward pointing unit normal to $\mathcal{C}_3$, and s is the arc length parameter. We also use the notation $x\cdot y$ in place of $\langle x,y\rangle$.

Consider for a moment the following problem: Given an *objective* curve, $\mathcal{M}$, which is the ZLS of a LSF $\Phi(x)$, and a parametrized family of level set functions, $\Psi(x;\lambda)$ with ZLS $\mathcal{L}(\lambda)$, find the value of the parameter vector λ such that $\mathcal{L}(\lambda)$ is closest to $\mathcal{M}$. Denote the distance between the parameter-dependent curve defined by $\Psi(x;\lambda)$ and the objective curve defined by $\Phi(x)$ by $\rho(\lambda)$. Then $\rho(\lambda) = (1/2)\int_{\mathcal{E}}\langle\mathcal{E},\nu\rangle\,ds$, where $\mathcal{E}$ is the ZLS of $\Theta(x;\lambda)$, defined as in the previous section. In order to apply gradient-based optimization methods, we must compute ρ_i, where subscript i denotes partial differentiation with respect to λ_i. This problem was addressed in [1]. Briefly summarizing that work, we have for the smooth segments of the curve $\rho_i(\lambda) = \int_{\mathcal{E}}\langle\mathcal{E}_i,\nu\rangle\,ds$. To obtain an expression for $\mathcal{E}_i$, consider the change in $\mathcal{E}$ corresponding to a change in the i-th parameter λ_i. We write $\Gamma(X(s;\lambda);\lambda) = 0$. So, $\Gamma_i + \langle\nabla\Gamma,\mathcal{E}_i\rangle = 0$. In fact, differentiation with respect to a parameter gives the same form found in the evolution equation, namely $\Gamma_i + \langle\mathcal{E}_i,\nu\rangle\|\nabla\Gamma\| = 0$. This time, however, the terms are arranged as $\langle\mathcal{E}_i,\nu\rangle = -\Gamma_i/\|\nabla\Gamma\|$. Making this substitution, we eventually obtain the following expression [1]: $\rho_i = -\int_{\mathcal{L}}\operatorname{sign}(\Phi)\Psi_i/\|\nabla\Psi\|\,ds$.

3 Parametrized Speed Functions

We return now to the problem of interest; that of estimating parameters in the speed function. The metric determining the distance between the obtained and target shapes is now $\rho(\lambda) := \rho(\Psi(T,x;\lambda),\Phi(T,x))$, with T a specified time, and $\Psi(T,x;\lambda)$ is the solution at time $t=T$ to the evolution equation $\Psi_t + \beta(\,\cdot\,;\lambda)\|\nabla\Psi\| = 0$, subject to $\Psi(0,x;\lambda) = \Psi_0(x)$. Note that now the λ dependence of Ψ is not due to an explicit parametriza-

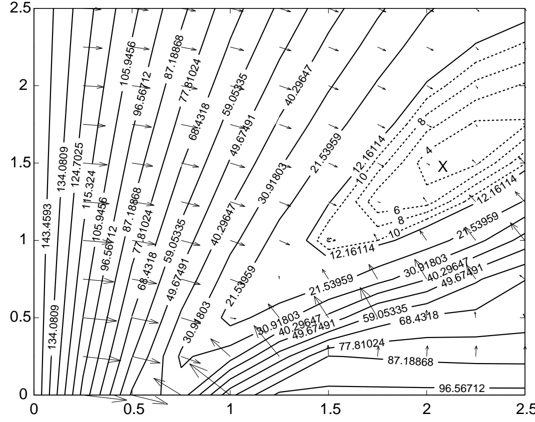

Figure 1: Cost contours for two parameter estimation problem with simulated measurement errors. '`X`' marks solution found by optimization scheme.

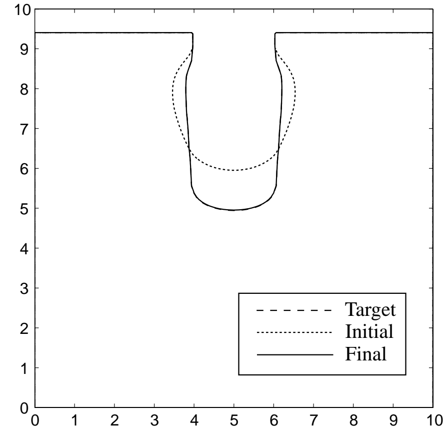

Figure 2: Estimation of two model parameters with a perfect model.

tion, but arises from the variation of β with λ in the evolution equation. Thus in the event that analytic gradients are desired, they must be determined somehow from knowledge of β. One way to accomplish this is to differentiate both sides of the evolution equation with respect to the i-th parameter. The result is a PDE for the gradient, coupled to the original evolution equation. This type of *sensitivity equation* approach is described further in [4].

We now restrict our attention to the plane, and consider speed functions of the form

$$\beta = \mu_1 \beta_0(x, y; \Lambda) + \mu_2 V(x, y; \Lambda) \cdot \nu \qquad (1)$$

This restriction is made for convenience in the choice of algorithms for the forward solution of the evolution equation. The form (1) is sufficiently general to handle the plasma etching process considered below. The first term in (1) is an isotropic component, where the parameter-dependent isotropic etch rate β_0 is allowed to vary with position. In the second term, a parameter-dependent vector V forms an inner product with ν, the outward-pointing unit normal to the surface. Thus, this term represents an orientation dependent component, where the orientation dependence can vary with position. With an eye towards our eventual chosen application, we refer to this term as the *sputtering* component. Note that the parameter vector λ has been partitioned into the parameters μ_1 and μ_2, which determine the relative contributions of the isotropic and sputtering components, and the process parameters Λ. Recall that the outward-pointing unit normal is given by $\nabla\Psi/\|\nabla\Psi\|$. Thus the evolution equation corresponding to speed function (1) is $\Psi_t + \mu_1\beta_0(x, y; \Lambda)\|\nabla\Psi\| + \mu_2 V(x, y; \Lambda) \cdot \nabla\Psi = 0$. This is a Hamilton-Jacobi equation with Hamiltonian $\mu_1\beta_0\|\nabla\Psi\| + \mu_2 V \cdot \nabla\Psi$, which may be shown to be convex. The third component of this equation is a linear advection term, in which the initial data "flows" with velocity $\mu_2 V$. To treat the non-convex case only the details of the numerical update scheme must be adjusted.

Now, take the derivative of the LSF evolution equation, exchange the order of differentiation, and denote sensitivity with respect to the μ or Λ by $S^{(q)}$. Then

$$\begin{aligned}
S_t^{(\mu_1)} + (\mu_1\beta_0\nu + \mu_2 V) \cdot \nabla S^{(\mu_1)} &= -\beta_0\|\nabla\Psi\| \\
S_t^{(\mu_2)} + (\mu_1\beta_0\nu + \mu_2 V) \cdot \nabla S^{(\mu_2)} &= -V \cdot \nabla\Psi \\
S_t^{(\Lambda_i)} + (\mu_1\beta_0\nu + \mu_2 V) \cdot \nabla S^{(\Lambda_i)} &= -(\mu_1\beta_{0i}\|\nabla\Psi\| \\
&\quad + \mu_2 V_i \cdot \nabla\Psi)
\end{aligned}$$

In deriving these equations, repeated use is made of the relation $\|\nabla\Psi\|_q = (1/\|\nabla\Psi\|)(\nabla\Psi \cdot \nabla\Psi_q) = \nu \cdot \nabla S^{(q)}$. These are first-order linear equations, in which the sensitivity is advected with velocity $(\mu_1\beta_0\nu + \mu_2 V)$ and sensitivity is "created" according to the various right-hand side reaction terms.

4 Example: An Ion-Assisted Etch Model

We now present an example of parameter estimation and process optimization for an ion-assisted etch. Here, a mask has been laid down and patterned, and the objective is to remove the material under the mask, down to a prescribed depth. This removal is accomplished through a combination of chemical reactions by neutral radicals and mechanical sputtering by charged ions. The wafer surface is modeled by three layers. At the lowest level is an inert planar substrate. Above this is the initially planar "active" layer, which is to be etched. At the top is the patterned mask, assumed here to be completely inert. The wafer surface is exposed to a plasma, which is composed of chemically active, but electrically neutral, radicals, and chemically inactive

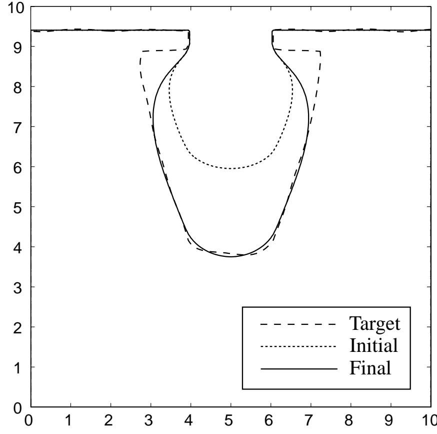

Figure 3: Estimation of two model parameters with an imperfect model.

ions. The ions are accelerated by the sheath potential, and after various momentum and charge interactions in the sheath, strike the exposed surface. The energy of impact varies over the points of the free surface, and is a function of position and orientation. We consider that two mechanisms may be at work. The first depends only on the radical concentration, which we assume to be homogeneous. This gives rise to an isotropic etching component. The second is associated with the incident ion energy, and may be due to mechanical sputtering or to enhancement of the chemical etch by the ion collision energy. We apply the speed function $\mu_1\beta_0(x,y) + \mu_2 V(x,y;\Lambda)\cdot\nu = 0$. This speed function is of the form (1), with β_0 and V spatially varying, but with β_0 independent of parameters. Here the full estimation problem is to recover the coefficients μ_1 and μ_2 governing the relative contributions of the isotropic and sputtering terms, respectively, and the parameters Λ that determine the vector field V. In this case V has the physical meaning of a normalized energy flux. The spatial dependence of the isotropic component is simple. The isotropic etch rate in the mask and substrate is zero, while in the active layer it is nominally one, scaled by μ_1. For a more complex spatial dependency see [3], where a process model for lithographic development was analyzed. This case included dependence of μ_1 on up to three parameters.

The details of the process model for the sputtering component are adapted from [10, 18, 19]. That model incorporates simplified versions of shadowing effects and scattering in the plasma sheath. The components of the flux vector, for etching of an infinite trench, are given at any point by

$$[V]_x = \int_\Omega j(\theta)\bar{E}(\theta)\sin^2\theta\cos\phi\, d\theta d\phi \qquad (2)$$

$$[V]_y = \int_\Omega j(\theta)\bar{E}(\theta)\cos\theta\, d\theta d\phi. \qquad (3)$$

Here the integral is taken over Ω, which is the solid angle over which the plasma is visible. The function $j(\theta)$ is the flux of particles moving with angle θ to the local vertical, and $\bar{E}(\theta)$ is the average energy of those particles. Note that all properties are assumed to be symmetric with respect to the local vertical, that is, independent of ϕ. Following [18], we set $\bar{E}(\theta) = \cos^2(\theta)$. Explicit computation of the flux vector is generally not possible, due to the term $j(\theta)$. Instead, write (2) and (3) as

$$[V]_x = \int_0^{\pi/2} Y(\theta)\sin\theta\cos\theta j(\theta)d\theta \qquad (4)$$

$$[V]_y = \int_0^{\pi/2} Z(\theta)\sin\theta\cos\theta j(\theta)d\theta \qquad (5)$$

where the integration over ϕ is carried out following [18], and the functions $Y(\theta)$ and $Z(\theta)$ contain all dependence on the geometry of the trench, while $j(\theta)$ contains all dependence on the plasma model. For the infinite trench, $Y(\theta)$ and $Z(\theta)$ can be computed in closed form, and are given by $X(\theta) = 2(\sin\phi_b - \sin\phi_a)\sin\theta\cos\theta$ and $Y(\theta) = 2(\pi - \phi_b - \phi_a)\cos^2\theta$, where ϕ_a and ϕ_b are the azimuthal visibility limits, for which formulas are given in [18]. The integrals (4) and (5) are approximated using the identity

$$\int_0^\theta \sin\theta\cos\theta j(\theta)d\theta = \frac{J}{2\pi}\exp(-\Lambda\bar{\sigma}_\theta). \qquad (6)$$

Here $\Lambda := 25.8E_{\text{lab}}^{-0.251}\delta D$, is a *single* parameter, with δ the number density of the plasma, D the effective thickness of the scattering region, and E_{lab} the ion energy in the laboratory frame. The function $\bar{\sigma}_\theta$ is the normalized total cross section for collison at angles greater than θ, and may be approximated by [10],

$$\bar{\sigma}_\theta \approx \begin{cases} \theta^{-0.251}(1-\theta/1.3); & 0 < \theta \le 1.3 \\ 0; & 1.3 < \theta \le \pi/2 \end{cases}. \qquad (7)$$

Then we have in an interval of width Δ_i centered on θ_i,

$$\begin{aligned} \chi_i &= \int_{\theta_i-\Delta_i/2}^{\theta_i+\Delta_i/2} \sin\theta\cos\theta j(\theta)d\theta \\ &= \tfrac{J}{2\pi}(\exp(-\Lambda\bar{\sigma}_{\theta_i+\Delta_i/2}) - \exp(-\Lambda\bar{\sigma}_{\theta_i-\Delta_i/2})). \end{aligned}$$

By evaluating the right hand side at intervals using (7), we generate a histogram. The histogram is used to evaluate (4) and (5) by assuming that $Y(\theta)$ and $Z(\theta)$ are constant in the interval $[\theta_i - \Delta_i/2, \theta_i + \Delta_i/2]$. Then $[\bar{V}]_x \approx \sum_i Y(\theta_i)\chi_i$ and $[\bar{V}]_y \approx \sum_i Z(\theta_i)\chi_i$. Here the overbar indicates that the constant term $J/2\pi$ has been absorbed into the parameter μ_2. We consider optimal estimation of model parameters from knowledge of the initial and final feature shape. The model is assumed to be as in the previous sections. Thus the parameters are μ_1, μ_2, and Λ.

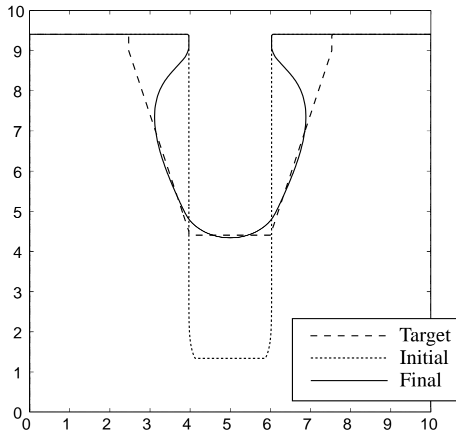

(a) Two parameters.

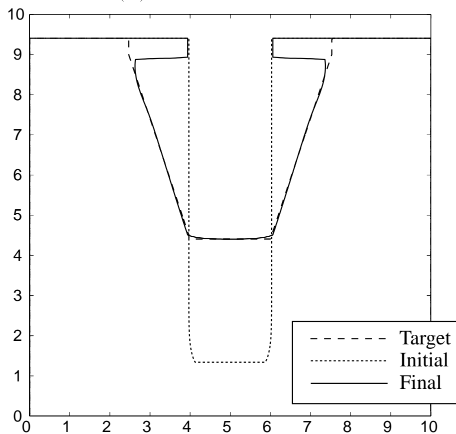

(b) Three parameters.

Figure 4: Optimal design of a sloped sidewalled channel.

As noted in [1], the template metric does not necessarily give a smooth cost function near the minimizer. For that reason the cost function chosen is $J = (1/2)\rho(\lambda)^2$. The gradient is then $\nabla J = \rho \nabla \rho$. This provides some smoothing when the optimal ρ is small, and allows us to use Hessian-based nonlinear programming methods such as sequential quadratic programming (SQP). The implementation of SQP used for this study was the Matlab Optimization Toolbox routine `fmincon` [5]. Lower bounds on the parameters are easily chosen; physical considerations dictate that the plasma parameter Λ can never be negative, and validity of the process model cannot be guaranteed if the rates μ_1 and μ_2 become negative. Thus the lower bounds for all three parameters were set to zero. No upper bound was placed on Λ, but μ_1 and μ_2 were limited to prevent numerical instability, and to minimize the possibility that the estimated surface would extend beyond the computational domain. The problem was scaled so that constraining the sum of μ_1 and μ_2 to be less than one would guarantee that the final feature would lie entirely within the computational domain. The actual upper bounds on μ_1 and μ_2 were usually set well above this level.

We consider first the estimation of two parameters, namely μ_2 and Λ. The primary purpose of the two parameter problem is to visualize the resulting cost function, and to show that the computed gradients are reasonable. One case was run in which the data was generated by the process model. In this case the model can perfectly capture the observed measurement, and the optimal value of the cost function is zero. In the second case, to simulate modeling errors, measurement errors, and other inaccuracies, the truth model was given a significant isotropic component, and the resulting data was then corrupted by a level set function consisting of several sinusoids with randomly generated phasing. We refer to these cases as "perfect" and 'imperfect" models, respectively. Figure 1 shows cost contours and gradients for the two parameter estimation problem corresponding to the imperfect model. Figure 2 shows an example of the results for the perfect model case. Figure 3 shows an example of the results for the imperfect model case. The analytically computed gradients seem consistent with the cost contours, and the results of the optimization scheme are generally quite good.

Next we consider optimal design. Here the target shape is a *desired* surface feature, and we view the parameters as control knobs which may be adjusted to produce this result. In the model being used these values are related to pressure, bias voltage, gas pressures, and other quantities that may indeed be specified by the process designer. The objective is to choose the settings that approximate the desired shape with minimal error. Once again only one target shape is used, because typically only the final shape is important to the process or device designer. The desired shape is known exactly, so measurement noise is not a factor. The same optimization settings were used here as in the model parameter estimation study of the previous section.

To test the algorithm, the desired topography is selected to be a channel with sloping sidewalls. This case was run for both two and three parameters. The results are shown in Fig. 4. The two parameter design does poorly. This is not unexpected, since the target design contains significant undercutting of the mask. On the other hand, the three parameter design, which includes an isotropic component capable of producing the desired undercut, does a nearly perfect job of achieving the target shape.

References

[1] J. M. Berg, K. Holmström, "On Parameter Estimation Using Level Sets," *SIAM Journal of Control and Optimization*, Vol. ,37,No. ,5, , pp. 1372–1393, 1999.

[2] J. M. Berg, A. Yezzi, and A. R. Tannenbaum,

"Curve Evolution Models for Real-Time Identification with Application to Plasma Etching," *IEEE Transactions Automatic Control*, *TAC*-44, No. 1, pp. 99–101, 1999.

[3] J. Berg, "Estimation of Parameter Values Appearing in Space and Orientation Dependent Curve Evolution Process Models," *Proceedings of the American Control Conference*, San Diego, CA, pp. 3905–3909, 1999.

[4] J. Borggaard and J. Burns, "A PDE sensitivity equation method for optimal aerodynanamic design," *Journal of Computational Physics*, **136** (2), pp. 366-384, 1997.

[5] T. F. Coleman, M. A. Branch and A. Grace, *Optimization Toolbox User's Guide, Version 2*, The MathWorks, Inc., Natick, MA, 1999.

[6] S. W. Butler, K. J. McLaughlin, T. F. Edgar, and I. Trachtenberg, "Development of techniques for real-time monitoring and control in plasma etching, II: multivariable control system analysis of manipulated, measured, and performance variables," *J. Electrochem. Soc.* **138**:9, pp. 2727-2735, 1991.

[7] T. S. Cale, M. B. Chaara, and A. Hasper, "Estimating Local Deposition Conditions and Kinetic Parameters Using Film Profiles," *Mat. Res. Soc. Symp. Proc.*, Vol. 260, pp. 393-398, 1992.

[8] G. P. Carnevale, P. Colpani, A. Marmiroli, A. Rebora, and A. Tixier, "Optimization of a Recessed LOCOS Using a Tuned 2-D Process Simulator," *Simulation of Semiconductor Devices and Processes Vol. 6*, H. Ryssel and P. Pichler, Eds., pp. 286–289, 1995.

[9] M. Hankinson, T. Vincent, K. B. Irani, and P. P. Khargonekar, "Integrated Real-Time and Run-to-Run Control of Etch Depth in Reactive Ion Etching," *IEEE Transactions on Semiconductor Manufacturing*, Vol. 10, No. 1, pp. 121–130, 1997.

[10] C. W. Jurgensen, "Sheath collision processes controlling the energy and directionality of surface bombardment in O_2 reactive ion etching," *J. Appl. Phys.*, **64**:2, pp. 590–597, 1988.

[11] K. J. McLaughlin, T. F. Edgar, and I. Trachtenberg, "Real-Time Monitoring and Control in Plasma Etching," *IEEE Control Systems Magazine*, pp. 3-10, April, 1991.

[12] C. J. Mogab, A. C. Adams, and D. L. Flamm, "Plasma Etching of Si and SiO_2s—The Effect of Oxygen Additions to CF_4 Plasmas," *J. Appl. Phys*, Vol. 49, No. 7, pp. 3796–3803, 1978.

[13] D. Mumford, "Mathematical Theories of Shape: Do They Model Perception?" *SPIE Vol. 1570 Geometric Methods in Computer Vision*, 1991.

[14] S.J. Osher and J.A. Sethian, "Fronts propagation with curvature dependent speed: Algorithms based on Hamilton-Jacobi formulations," *Journal of Computational Physics* **79**, pp. 12-49, 1988.

[15] B. A. Rashap, M. E. Elta, H. Etemad, J. P. Fournier, J. S. Freudenberg, M. D. Giles, J. W. Grizzle, P. T. Kabamba, P. P. Khargonekar, S. Lafortune, J. R. Moyne, D. Teneketzis, and F. L. Terry, "Control of semiconductor manufacturing equipment: real-time feedback control of a reactive ion etcher," *IEEE Trans. Semiconduct. Manufacturing* **8**:3, pp. 286-297, 1995.

[16] J. A. Sethian, *Level Set Methods and Fast Marching Methods: Evolving Interfaces in Geometry, Fluid Mechanics, Computer Vision, and Materials Science*, second edition, Cambridge University Press, 1999.

[17] J. A. Sethian and D. Adalsteinsson, "An Overview of Level Set Methods for Etching, Deposition, and Lithography Development," *IEEE Trans. Semiconduct. Manufacturing* **10**:1, pp. 167–184, 1997.

[18] E. Shaqfeh and C. Jurgensen, "Simulation of reactive ion etching pattern transfer," *J. Appl. Physics*, **66**, pp. 4664–4675, 1989.

[19] V. Singh, E. Shaqfeh, and J. McVittie, "Simulation of profile evolution in silicon reactive ion etching with re-emission and surface diffusion," *J. Vac. Technol. B*, **10**, pp. 1091–1104, 1992.

[20] D. Stokes and G. May, "Real-Time Control of Reactive Ion Etching Using Neural Networks," *Proccedings of the American Control Conference*, Albuquerque, NM, pp. 1575–1578, 1997.

[21] S. Tazawa, S. Matsuo, and K. Saito, "A General Characterization and Simulation Method for Deposition and Etching Technology," *IEEE Transactions on Semiconductor Manufacturing*, Vol. 5, No. 1, pp. 27–33, 1992.

[22] T. L. Vincent, P. P. Khargonekar, F. L. Terry, Jr., "An Extended Kalman Filtering-Based Method of Processing Reflectometry Data for Fast *In Situ* Etch Rate Measurements," *IEEE Transactions on Semiconductor Manufacturing*, Vol. 10, No. 1, pp. 42–51, 1997.

[23] E. Zawaideh and N. S. Kim, "A plasma etching model based on a generalized transport approach," *J. Appl. Phys.*, Vol. 62, No. 15, pp. 2498–2507, 1987.

[24] E. Zawaideh and N. S. Kim, "A generalized plasma etching model," *J. Appl. Phys.*, Vol. 64, No. 8, pp. 4199–4207, 1988.